Int. J. Solids Structures, 1972, Vol. 8, pp. 511 to 531. Pergamon Press. Printed in Great Britain

A PROCEDURE FOR DETERMINING THE CONSTITUTIVE EQUATIONS FOR MATERIALS EXHIBITING BOTH TIME-DEPENDENT AND TIME-INDEPENDENT PLASTICITY

N. CRISTESCU†

Faculty of Mathematics and Mechanics, University of Bucharest, Bucharest, Romania

Abstract—A procedure is given in order to determine various functions and constants entering in a constitutive equation exhibiting both time-dependent and time-independent plasticity, starting from a set of experimental data. As typical experiments one has chosen the symmetric longitudinal impact of two identical bars, since for such kinds of problems a great deal of experimental data are available.

The unloading process is also considered since it is mainly during unloading that interesting aspects concerning "plasticity" may be put into evidence. A "relaxation boundary" which plays a main role in time-dependent plasticity is introduced. Several computed examples are given in order to show the influence of various functions or constants entering in the constitutive equation.

INTRODUCTION

THE main objective of the present paper is to give a procedure to be followed in order to determine a constitutive equation exhibiting both time-dependent and time-independent plasticity when starting from a set of experimental data. The discussion is restricted to a one-dimensional problem for which a great deal of experimental data are available and for which the analytical approach is quite simple. This is the symmetric impact of two identical finite bars. This problem was considered in [1, 2] by using a constitutive equation written in finite form. The experimental data used in the present paper are due to Bell (see [2]).

In order to make the discussion as complete as possible we have started by solving the same problem (same boundary and initial conditions) by using some constitutive equations written in finite form which have been recommended for the same specific material. The numerical examples were computed for a certain kind of aluminum (commercial purity dead annealed 1100°F aluminum, annealed for 2 hr at 1100°F and furnace cooled). For this particular material Bell‡ has suggested the following stress–strain relation to be used during loading in "quasi-static" tests

$$\sigma = 3{\cdot}32\times 10^4\varepsilon^{\frac{3}{8}} \tag{1}$$

where the stress σ is given in psi and $\varepsilon = \partial u/\partial x$ is a finite strain measure, u is longitudinal displacement and x is material coordinate. From dynamic tests Bell [3] comes to the

† Graduate Research Professor, Department of Engineering Science and Mechanics, University of Florida, Gainesville, Florida.

‡ Private communication.

conclusion that for the same material the following parabolic law is to be used during dynamic loading

$$\sigma = \beta \varepsilon^{1/\alpha} \tag{2}$$

with $\beta = 5{\cdot}6 \times 10^4$ psi and $\alpha = 2$.

In order to take into account the elastic properties as well (1) has been written for the loading process in the form

$$\begin{aligned} \sigma &= E\varepsilon && \text{if } \sigma \leq \sigma_{Y0} \\ \sigma &= 3{\cdot}32 \times 10^4 \varepsilon^{\frac{1}{2}} && \text{if } \sigma \geq \sigma_{Y0} \end{aligned} \tag{3}$$

with $E = 10{\cdot}2 \times 10^6$ psi (717,000 kg/cm^2) and $\sigma_{Y0} = 1068{\cdot}24$ psi (75·11 kg/cm^2). The yield stress is not exactly the one found in static tests, which is $\sigma_Y = 1100$ psi (77·34 kg/cm^2), but is the stress corresponding to the point of intersection of the two curves (3).

In a similar manner when starting from the dynamic law (2) we have written the stress–strain relation in the form

$$\begin{aligned} \sigma &= E\varepsilon && \text{if } \sigma \leq \sigma_{Y1} \\ \sigma &= \beta \varepsilon^{1/\alpha} && \text{if } \sigma \geq \sigma_{Y1} \end{aligned} \tag{4}$$

with this time $\sigma_{Y1} = 307{\cdot}5$ psi (21·62 kg/cm^2). Since this value of the yield stress is much too low, besides (4) in the computation we have used also

$$\begin{aligned} \sigma &= E\varepsilon && \text{if } \sigma \leq \sigma_{Y2} \\ \sigma &= \beta(\varepsilon + \varepsilon_0)^{1/\alpha} && \text{if } \sigma \geq \sigma_{Y2} \end{aligned} \tag{5}$$

with $\sigma_{Y2} = 1100$ psi (77·34 kg/cm^2)—the yield stress found in static experiments—and $\varepsilon_0 = 0{\cdot}000278$.

Another attempt used to match a much higher yield point with the parabolic law (4) was to consider that the stress–strain curve is composed of three parts: the Hooke's law, then a straight line passing through the yield point and tangent to the parabola (2) and for higher strains by (2) itself [see (10) below].

The specific problem for which the computation have been done is the symmetric impact of two identical aluminum bars of finite length. One has assumed that one of the bars, the specimen, is for $t < 0$ at rest and undeformed while the other bar, the hitter, is impacting at $t = 0$ the first one with a certain initial velocity V. The impact velocity in most of the cases was the same $V = 1600$ in./sec (40·64 m/sec). For details concerning the procedure to be used when the stress–strain law is of the form (4) or (5) see [1, 2]. The way in which the variation of the Young's modulus with the plastic strain may influence the unloading process was analysed in [4].

THE CONSTITUTIVE EQUATION

A constitutive equation of the type introduced in [6]:

$$\frac{\partial \varepsilon}{\partial t} = \frac{1}{E}\frac{\partial \sigma}{\partial t} + \Phi(\sigma, \varepsilon)\frac{\partial \sigma}{\partial t} + \Psi(\sigma, \varepsilon) \tag{6}$$

has been used in the plastic domain (for more qualitative details see [5, chapter III]). The word "plastic" is used here in a general sense, time effects being included as well.

The time dependent properties are described by the function $\Psi(\sigma, \varepsilon)$ which in the present paper was chosen to depend in a linear manner on the "overstress" $\sigma - f(\varepsilon)$:

$$\Psi(\sigma, \varepsilon) = \begin{cases} \dfrac{k(\varepsilon)}{E}[\sigma - f(\varepsilon)] & \text{if } \sigma > f(\varepsilon) \text{ and } \varepsilon \geq \varepsilon_Y \\ 0 & \text{if } \sigma \leq f(\varepsilon) \text{ or } \varepsilon < \varepsilon_Y \end{cases} \tag{7}$$

where

$$\sigma = f(\varepsilon) \tag{8}$$

represents in a stress–strain plane a plastic/elastic boundary, i.e. for $\sigma > f(\varepsilon)$ the response is plastic and elastic while for $\sigma < f(\varepsilon)$ the response of the material is elastic only. This curve may be called "the relaxation boundary" since above this curve the model allows dynamic stress-relaxation, while under it no relaxation takes place, and the only response is the elastic one (see Fig. 1). Generally (8) does not coincide with what is generally called the "quasistatic" stress–strain curve, though for some specific materials it may coincide. The "yield point" may also differ from the quasistatic one as well.

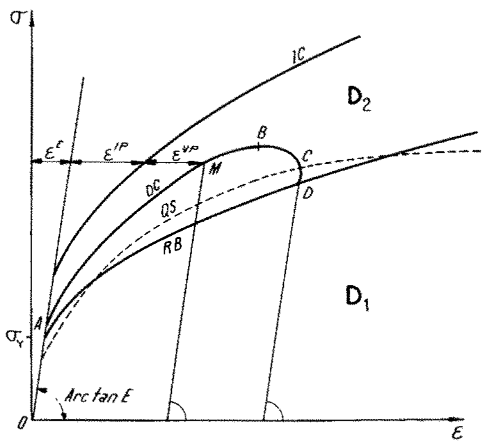

FIG. 1. Various significant stress–strain curves: *RB*, relaxation boundary; *QS*, quasistatic stress–strain curve; *DC*, typical dynamic stress–strain curve; *IC*, instantaneous curve; D_1, elastic domain; D_2, domain of possible dynamic stress and strain states.

In the present paper the following expressions for $f(\varepsilon)$ have been used, both based on interpreting Bell's "dynamic stress–strain curve" as a relaxation boundary, but correcting the behavior near the yield point in two different ways:

$$f(\varepsilon) = \begin{cases} \sigma_Y & \text{if } \varepsilon \leq \varepsilon_Y \\ \beta(\varepsilon + \varepsilon_0)^{1/\alpha} & \text{if } \varepsilon \geq \varepsilon_Y \end{cases} \tag{9}$$

with α, β and ε_0 constants, and

$$f(\varepsilon) = \begin{cases} \sigma_Y & \text{if } \varepsilon \leq \varepsilon_Y \\ \sigma_Y + \dfrac{\beta}{2}\varepsilon_z^{-1/2}(\varepsilon - \varepsilon_Y) & \text{if } \varepsilon_Y \leq \varepsilon \leq \varepsilon_z \\ \beta\varepsilon^{1/2} & \text{if } \varepsilon_z \leq \varepsilon \end{cases} \tag{10}$$

where

$$\varepsilon_z = \left(\frac{\beta\varepsilon_Y}{\sigma_Y - \sqrt{(\sigma_Y^2 - \varepsilon_Y\beta^2)}}\right)^2. \tag{11}$$

Thus by introducing (10) the curve (8) was approximated by two segments of straight lines, continued by parabola (2). The two straight lines are the Hooke's law and respectively the straight line tangent to (2) and passing through the yield point. This procedure allowed the raising of the yield point up to the desired position obtained experimentally.

The function $k(\varepsilon)$ (the expression $E/k(\varepsilon)$ may be interpreted as a variable viscosity coefficient) was taken in the form

$$k(\varepsilon) = k_0\left[1 - \exp\left(-\frac{\varepsilon}{\hat{\varepsilon}}\right)\right] \tag{12}$$

with k_0 and $\hat{\varepsilon}$ constants. In some cases one has assumed simply that

$$k = k_0 = \text{const.} \tag{13}$$

In other cases $\hat{\varepsilon}$ was chosen so that most of the variation in $k(\varepsilon)$ occurred between the yield strain ε_Y and $10\varepsilon_Y$ and k was nearly constant during the major part of the plastic straining.

In (6) the function Φ is the measure of the "instantaneous plastic response" of the material, that is $1/(\Phi + 1/E)$ is the slope of the dynamic stress–strain curve of instantaneous response (Fig. 1). Therefore $\Phi(\partial\sigma/\partial t)$ is the "time-independent" component of the rate of strain, in the sense of classical plasticity theory; this makes clear the meaning of the term "instantaneous" which is used here for convenience. Several expressions for Φ have been used in the numerical examples. For relaxation boundaries of the form (9) these were chosen to satisfy the inequality

$$1 \geq \frac{1}{E\Phi + 1} > \frac{1}{\alpha(\varepsilon + \varepsilon_0)}\left(\frac{\sigma}{E} - \frac{\Psi}{k}\right) \tag{14}$$

for any stress and strain states in the loading domain (i.e. when $\Psi \neq 0$) and to fit as well as possible the experimental data. The inequality (14) expresses the assumption that the slope of the instantaneous stress–strain curve is comprised between the elastic one and that furnished by the relaxation boundary (8) for the same strain. The inequality (14) is a "sufficient" one though one may contemplate to establish a weaker one if necessary (mainly in what concerns the second inequality).

The function Φ could be determined from the speed of the acceleration waves, since Φ enters the expression for the characteristic speed c in (28) below. Since experimental acceleration wave speed data for the whole loading range were not available, a simple function was chosen for a first approximation to the "instantaneous-response curve", whose slope is $1/(\Phi + 1/E)$, and it was found that a good representation of the propagation of the rising part of the strain–time curve could be obtained by adjusting slightly the function Φ. Two forms were used, both initially based on a cubic parabola for the instantaneous response curve: $\varepsilon = A\sigma^3$ suggested equation (19) below, while $(\sigma - \sigma_Y) = B(\varepsilon - \varepsilon_Y)^{\frac{1}{3}}$ suggested equation (15). In each case the resulting expression for Φ was then further adjusted by making the constant A or B a slowly varying function of ε in order to decrease the importance of Φ at the higher strains. In (15) there has also been introduced a threshhold overstress σ^* as indicated in (17) and (18), below which $\Phi = 0$.

One of the expressions used for Φ is

$$\Phi(\varepsilon) = \chi \left\{ \frac{3[\varepsilon - \varepsilon_Y - \varepsilon^* + (a/3E)^{\frac{3}{2}}]^{\frac{2}{3}}}{a} - \frac{1}{E} \right\} \tag{15}$$

with

$$a = m + n\sqrt{\varepsilon} \tag{16}$$

where m and n are constants. χ is a parameter which plays an important role in the program. It is defined for a single loading–unloading cycle by

$$\chi = \begin{cases} 0 & \text{if } \sigma \leq f(\varepsilon) + \sigma^* \quad \text{or } \dfrac{\partial \sigma}{\partial t} < 0 \\ \\ 1 & \text{if } \sigma > f(\varepsilon) + \sigma^* \quad \text{and } \dfrac{\partial \sigma}{\partial t} > 0. \end{cases} \tag{17}$$

In most of the cases considered one has taken $\sigma^* = E\varepsilon^* = 0$; however, the case

$$\frac{\sigma^*}{E} = \varepsilon^* = h + \lambda \left[\varepsilon - f^{-1}\left(\frac{\sigma_Y}{E} + h \right) \right] \tag{18}$$

was considered as well. Here h and λ are constants.

Another expression used for Φ was

$$\Phi(\sigma, \varepsilon) = \chi \frac{\gamma}{E} \left[3 \left(\frac{E}{p + q\sqrt{\varepsilon}} \right)^3 \left(\frac{\sigma}{E} \right)^2 - 1 \right] \tag{19}$$

where γ, p and q are constants. In particular by making $\gamma = 0$ one has considered the case

$$\Phi = 0 \tag{20}$$

which corresponds to the Malvern [7] model.

The function Φ as given by (15) was chosen so that at $\varepsilon = \varepsilon_Y + \varepsilon^*$ we have $\Phi = 0$ while further on for increasing ε the function Φ increases. This function plays an important role during the period of increasing stress. We remember that always $\Phi \geq 0$.

Thus in the present paper the explicit expression for Φ was determined mainly from considering the variation in time of the strain at various sections of the bar. However, the function Φ is responsible for the maximum stress reached in dynamic loading at various sections of the bar. By knowing the stress variation in a single section, at the impacted end, one can uniquely determine Φ. By diminishing Φ the maximum stress increases.

Generally, trying to find appropriate expressions for the functions Φ and Ψ one has used mainly the variation in time of the strain at various sections of the bar, since they seem to be the most accurately established (with diffraction grating technique) from all the other experimental data available. The other experimental data were used mainly for a cross check.

The parameter which plays a dominant role in the description of the time-dependent properties [function $\Psi(\sigma, \varepsilon)$] is the function $k(\varepsilon)$. If k is very small, the stress–strain curves at all sections of the bar will approach the instantaneous-response curve defined by

$$\frac{d\sigma}{d\varepsilon} = \frac{1}{\Phi + 1/E}. \tag{21}$$

If k is very big, most of these curves (maybe with the exception of the sections very close to the impacted end) will significantly approach the relaxation boundary (8). In this last case, in order to have smaller computational errors, it is better to use the relaxation boundary as a finite stress–strain law and to use an appropriate program. The same is true for very small values of k: one can use the instantaneous-response curve as a stress–strain law written in finite form.

Figure 1 shows the various significant curves and domains in the $\sigma \sim \varepsilon$ plane. D_1 is the elastic domain. The points in D_2 are all possible stress and strain states which can be reached in dynamic experiments. These two domains are separated by the relaxation boundary while the upper boundary for D_2 is the instantaneous response curve. A typical dynamic stress–strain curve is also shown. At a certain point M the total strain is a sum of three components: the elastic one ε^E, the time-independent plastic one ε^{IP} and the time-dependent plastic one ε^{VP}. In order to simplify the notations below one will use the notation $\varepsilon^P = \varepsilon^{IP} + \varepsilon^{VP}$.

In order to make precise the terminology used, we will call *loading* the states (of stress, strain and rate of strain) which satisfy $\Phi > 0$ and $\Psi > 0$ (segment AB in Fig. 1). These will be denoted by L. The states satisfying $\Phi = 0$ and $\Psi > 0$ will be called *relaxation* and will be denoted by R (BD in Fig. 1). Finally the states satisfying $\Phi = 0$ and $\Psi = 0$ (all points in domain D_1) will be called *unloading* (or elastic) and will be denoted by U. In fact it is only in point C where $\dot{\varepsilon} = 0$ that a pure relaxation takes place; this is an unstable situation. In D, $\dot{\varepsilon}^P = 0$ and sometimes even $\dot{\varepsilon} = 0$, the situation being often stable (see [5]).

Thirteen different models were examined (see Table 1). In models I–III, $\Psi = 0$ and a classical plasticity formulation was used. In VIII, $\Phi = 0$, i.e. a Malvern-type law is considered. The other nine models offer various combinations of Φ and Ψ. In model I the "quasistatic" stress–strain curve was used, while in XI this curve was considered to be the relaxation boundary towards which the stress relaxes. In models II and III two variants of the "dynamic" finite form stress–strain law is used. Then (4) was used as a relaxation boundary in example XI, while (5) was used as relaxation boundary in examples VII–IX and X. Finally in examples IV–VI, XII and XIII the relaxation boundary is of the form (10).

FORMULATION OF THE PROBLEM

Besides the constitutive equation (6) we have the equation of motion

$$\rho \frac{\partial v}{\partial t} = \frac{\partial \sigma}{\partial x} \tag{22}$$

TABLE 1

No. of example	Formulas used	Constants used
I	(3)	$\sigma_Y = 1068$ psi, $\varepsilon_Y = 0{\cdot}0001047$
II	(4)	$\sigma_Y = 307{\cdot}5$ psi, $\varepsilon_Y = 0{\cdot}00003014$
III	(5)	$\sigma_Y = 1100$ psi, $\varepsilon_Y = 0{\cdot}00010789$, $\varepsilon_0 = 0{\cdot}0002779$
IV	(7), (10), (12), (15), (16)	$\sigma_Y = 1500$ psi, $\varepsilon_Y = 0{\cdot}000147059$, $\varepsilon_Z = 0{\cdot}002575$, $k_0 = 10^3\ \mathrm{sec}^{-1}$, $\hat{\varepsilon} = 0{\cdot}0004$, $\varepsilon^* = 0$, $m = 3{\cdot}25\times10^4$ psi, $n = 9\times10^4$ psi
V	Same as IV	Same as IV, *but* $n = 20\times10^6$
VI	Same as IV	Same as IV, *but* $k_0 = 3\times10^2$
VII	(7), (9), (19)	$\sigma_Y = 1100$ psi, $\varepsilon_Y = 0{\cdot}0001078$, $\varepsilon_0 = 0{\cdot}0002779$, $\alpha = 2$, $\beta = 5{\cdot}6\times10^4$ psi, $k = 10^3\ \mathrm{sec}^{-1}$, $\gamma = 1$, $p = 3{\cdot}25\times10^4$ psi, $q = 2\times10^4$ psi
VIII	Same as VII	Same as VII, *but* $\gamma = 0$
IX	Same as VII	Same as VII, *but* $k = 10\ \mathrm{sec}^{-1}$
X	(7), (9), (12), (15), (16)	$\sigma_Y = 1224$ psi, $\varepsilon_Y = 0{\cdot}000120$, $\varepsilon_0 = 0{\cdot}0003577$, $\alpha = 2$, $\beta = 5{\cdot}6\times10^4$ psi, $k_0 = 10^3\ \mathrm{sec}^{-1}$, $\hat{\varepsilon} = 0{\cdot}0004$, $m = 3{\cdot}25\times10^4$ psi, $n = 9\times10^4$ psi, $\varepsilon^* = 0$
XI	(7), (9), (19)	$\sigma_Y = 1068$ psi, $\varepsilon_Y = 0{\cdot}0001047$, $\varepsilon_0 = 0$, $\alpha = \frac{8}{3}$, $\beta = 3{\cdot}32\times10^4$ psi, $k = 10^3\ \mathrm{sec}^{-1}$, $\gamma = 1$, $p = 3{\cdot}25\times10^4$ psi, $q = 0$
XII	(7), (10), (12), (15), (16), (18)	$\sigma_Y = 1500$ psi, $\varepsilon_Y = 0{\cdot}000147059$, $\varepsilon_Z = 0{\cdot}002575$, $\alpha = 2$, $\beta = 5{\cdot}6\times10^4$ psi, $k_0 = 10^3\ \mathrm{sec}^{-1}$, $\hat{\varepsilon} = 0{\cdot}0004$, $m = 3{\cdot}25\times10^4$ psi, $n = 9\times10^4$ psi, $h = 0{\cdot}000004$, $\lambda = 0{\cdot}00005$
XIII	Same as XII	Same as XII, *but* $k_0 = 10^2\ \mathrm{sec}^{-1}$

and the compatibility equation

$$\frac{\partial v}{\partial x} = \frac{\partial \varepsilon}{\partial t} \tag{23}$$

where v is the particle velocity and ρ the mass density.

The system (6), (22) and (23) is a hyperbolic one, with the characteristic lines ([5, chapter III])

$$\begin{aligned} \mathrm{d}x &= \pm c(\sigma, \varepsilon)\,\mathrm{d}t \\ \mathrm{d}x &= 0 \end{aligned} \tag{24}$$

along which are satisfied the differential relations

$$\mathrm{d}\sigma = \mp \rho c\,\mathrm{d}v + \rho c^2 \Psi\,\mathrm{d}t \tag{25}$$

and

$$\begin{aligned} \mathrm{d}\varepsilon_E &= \frac{1}{E}\mathrm{d}\sigma \\ \mathrm{d}\varepsilon_P &= \Phi(\sigma, \varepsilon)\,\mathrm{d}\sigma + \Psi(\sigma, \varepsilon)\,\mathrm{d}t, \end{aligned} \tag{26}$$

respectively. One has used also the relation

$$\frac{\partial \varepsilon}{\partial t} = \frac{\partial \varepsilon_E}{\partial t} + \frac{\partial \varepsilon_P}{\partial t} \tag{27}$$

where ε_E and ε_P denote elastic and total plastic strains while the elastic, reversible part of the strain, is defined by introducing the concept of instantaneous unloading.

In (23) the velocity of propagation $c(\sigma, \varepsilon)$ is furnished by

$$c = \frac{c_0}{\sqrt{(1+E\Phi)}} \tag{28}$$

where

$$c_0 = \sqrt{\frac{E}{\rho}} \tag{29}$$

is the elastic "bar" velocity.

The initial conditions are:

$$\left.\begin{matrix} t = 0 \\ 0 \leq x \leq l \end{matrix}\right\} : \sigma = v = \varepsilon = 0 \tag{30}$$

with l the initial length of the bar.

As for the boundary conditions, the end $x = l$ of the bar is free,

$$\left.\begin{matrix} x = l \\ t \geq 0 \end{matrix}\right\} : \sigma = 0. \tag{31}$$

For the impacted end we assume that at $t = 0$ the hitter impacts the specimen with the velocity V. Three time periods will be distinguished (t is given in μsec):

$$x = 0 \quad \text{and} \quad \begin{cases} 0 \leq t \leq 10\ \mu\text{sec}: & v = \dfrac{V}{10}t \\ 10\ \mu\text{sec} \leq t \leq T_c: & v_{\text{specimen}} = v_{\text{hitter}} \\ T_c \leq t: & \sigma = 0 \end{cases} \tag{32}$$

where T_c is the time of contact between the two bars. The time of contact results from the computations. In order to simplify the computer program the sudden impact is handled in the computation by a fast, but smooth variation of the impact velocity within 10 μsec. Thus "shock waves" were not considered in the present paper. The second condition (32) is simply a symmetry condition, i.e. at the impacted end the two bars move with the same velocity. The magnitude of this velocity is obtained by computations.

The method used to integrate the previously mentioned equations is the method of characteristics. The mesh size was generally $2\,\Delta t = 0{\cdot}5\ \mu$sec, but in the triangle bounded by

$$x = 0, \qquad x = c_0 t \quad \text{and} \quad x = -c_0(t-20\ \mu\text{sec}) \tag{33}$$

the mesh was taken up to ten times smaller. The computations have been carried out in dimensionless variables in a manner similar to that described in [1].

DISCUSSION OF NUMERICAL EXAMPLES

Ten examples (see Table 1) have been computed using various expressions for the functions Φ and Ψ entering in (6). These were compared with the results obtained by using same stress–strain laws written in finite form as given by formulas (3)–(5) and with some experimental data available. Some of the computed results are listed in Table 2. The cases computed by using stress–strain laws written in finite form were obtained by assuming for boundary conditions an instantaneous impact, i.e. the first elastic wave is a shock wave, etc. (see [1, 2]). For the cases IV–XIII however we have assumed (32) as boundary condition.

TABLE 2

No. of example	σ_{max} (psi)		ε_{max}		T_c	v_f	$\bar{\varepsilon}$	Penetration of first unloading region, x_U
	Peak	Plateau	$x = 0$	Plateau	(μsec)	(in./sec)	$x = D/2$	
I	None	8000	0·0225	0·0225	307·5	834·9	—	4·5D
II	None	8320	0·0221	0·0221	307·5	896·4	—	5·75D
III	None	8450	0·0225	0·0225	307·5	895·1	—	4·25D
IV	9269	8357	0·0224	0·0224	309·9	896·7	0·0127	4·5D
V	9859	8400	0·0226	0·0226	304·5	906·0	0·0106	4·75D
VI	9976	—	0·0228	—	300·3	895·3	0·0125	5·0D
VII	9182	8450	0·0230	0·0225	303·3	904·1	0·0116	5·25D
VIII	14,052	~8500	0·0231	0·0230 ~ 0·0227	295·1	911·7	0·0065	5·75D
IX	9567	9460	0·0219	0·0215	279·2	903·2	0·0111	7·0D
X	9256	8400	0·0223	0·0223	307·2	898·0	0·0126	5·0D
XI	8973	~8290	0·0252	0·0247	305·1	898·3	0·0108	5·5D
XII	9276	8360	0·0225	0·0224	309·8	898·2	0·0127	4·5D
XIII	10,320		0·0225		285·4	901·6	0·0122	5·75D
Experimental		8300		0·0219	310·8	891	0·0135	4 ~ 5D

In Table 2 are listed the numerical values of some quantities which can be quite precisely established both theoretically and experimentally. Those are the time of contact between the two bars T_c, the final velocity of the specimen v_f and the strain $\bar{\varepsilon}$ corresponding to the maximum of the surface angle (see [3]) at the section $x = D/2$ of the bar (this maximum occurs at the point where the strain–time curves are changing curvature). The final velocity was computed as the average velocity of the specimen after rebound. Comparing the computed values of T_c, v_f and $\bar{\varepsilon}$ with the experimental one, one can conclude that some of the examples are in good agreement with the experimental data, especially IV, XII, X and VII.

Generally:

T_c decreases when Φ decreases and decreases significantly with Ψ;

v_f, however, increases when Φ decreases, but decreases with Ψ;

$\bar{\varepsilon}$ decreases significantly with Φ and slightly decreases with Ψ.

The section of the rod up to where the first unloading region penetrates into the loading region is not measured experimentally with the same accuracy. However, the experimental value $x_U = 4 \sim 5D$ is met by several of the examples, mainly by XII, IV, V and III. The value of x_U is governed mainly by the magnitude of the yield stress.

In example I the static stress–strain law (3) was used. The computations were carried out with a program similar to the one described in [1]. The variations of various required functions either in time or along the bar were compared with the experimental data. The solution obtained is in poor agreement with the experimental data. This was evident mainly from the comparison of the graphs showing the variation in time of the strain at various sections of the bar as furnished by the example I and the experimental data. The main discrepancies seems to be in the arrival time of the loading waves, the maximum strain at various sections and the overall poor description of the strain variation near the free end of the bar.

In example XI one has considered the static stress–strain curve to be the curve (8) towards which the relaxation takes place. The solution obtained seems again to be in poor agreement with the experimental data, and as a whole has a rather close resemblance with the solution obtained with the quasistatic finite stress–strain law (3). The maxima of the strains near the impacted end are much too high, while near the free end they are much too low. Thus it was shown that for the material considered the quasistatic stress–strain curve is not appropriate to be used as relaxation boundary.

Example IV was computed by using (10) for relaxation boundary. As for the function Φ, the expression (15) was used. According to this expression, at the beginning of the plastic deformation, near the yield point, Φ is zero and then increases as strain increases. Example IV gives a quite good agreement with most of the experimental data. See especially the strain–time curves in Fig. 2.

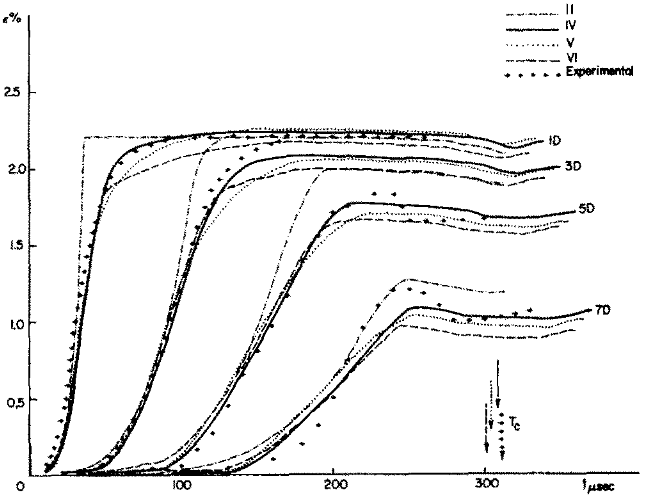

FIG. 2. Comparison between strain–time curves as obtained with finite stress–strain law (II), rate-type laws (IV–VI) and experimental data (1D means "one diameter from the impacted end", etc.).

Examples V and VI use the same basic model as IV, but with one of the main constants varied in each case to show how it affects the solution. In V, the value of n was increased, thus decreasing everywhere the value of Φ. This decrease was more significant for higher strains. In a similar manner the example VI was computed for the same constants as in IV except for a smaller value of k_0.

Comparisons will be made with the experimental data and also with computed cases obtained with the finite-form stress–strain laws, examples II and III. Example II is best for comparison in the major part of the solution, since it is based on the curve (2) which also forms the greater part of the relaxation boundary (8). Near the free end, however, while the stresses are still near the yield stress, example III is more suitable for comparison, since it assumes a higher and more reasonable value for the yield stress.

An overall description of the obtained solution may be read on the characteristic plane. Two such characteristic planes are shown in Figs. 3 and 4 for the cases IV and VI, respectively. The loading, unloading and relaxation domains are denoted by L, U and R, respectively. The R/U boundary is shown by a solid curve and the L/R boundary by a dotted curve (except where it coincides with R/U). In each case the boundary points are part of the regions enclosed. The first elastic wave which reflects at 50 μsec from the free end will penetrate into the L region as an unloading wave. This first penetration of the unloading domain into the loading region has been observed experimentally to stop somewhere between 4 and 5 diameters. The same was obtained for most of the examples shown

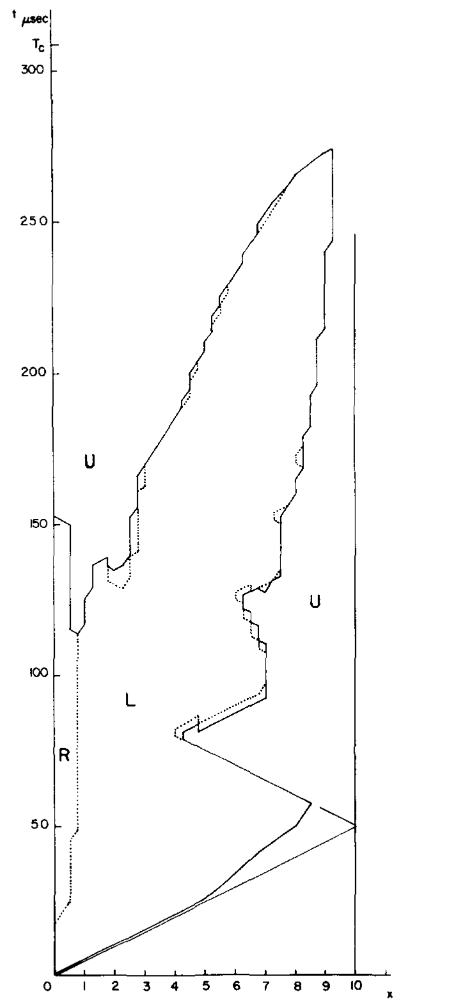

FIG. 3. Characteristic plane for example IV showing loading (L), unloading (U) and relaxation (R) regions.

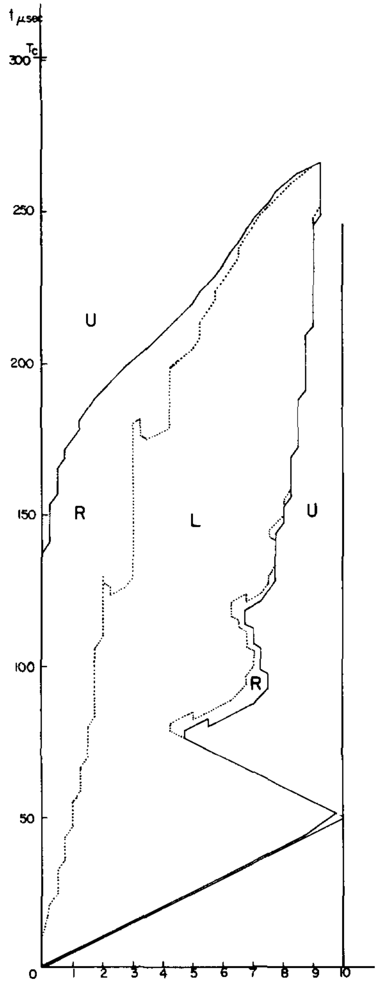

Fig. 4. Characteristic plane for example VI showing the increase of the R-regions when the value of k is decreased.

here. The characteristic plane for the example V was not given since it resembles the one shown in Fig. 3. A comparison of the two characteristic planes with the characteristic planes for examples II and III (given in [2]) furnishes the following. The part of the U-region near the free end in Fig. 3 has a shape close to that of example III, though a little wider, because in example IV the yield stress is slightly higher than in example III. (It is mainly the yield stress which governs the shape of this part of the unloading region.) The left side of the U-region, the one near the impacted end, is distinct from that of example III. In examples IV–VI the unloading process near the impacted end starts much later than in examples III and II.

Figure 2 shows the variation in time of the strain at various sections of the bar as obtained from IV–VI and from experiment. The solution II was given as well. The effect of the overall reduction of Φ can be seen following the solution given by V and comparing it with IV. With example V, the arrival times of the first part of the rising portion of the ε–t curves are too early; an opposite effect is to be seen at the upper part of these curves. The maxima of the strains at various sections become smaller than in IV mainly near the free end, but slightly higher near the impacted end. Finally the time of contact slightly decreases. Turning now to the example VI, one notes first a significant decrease of the strain maxima and that of the time of contact. A slight reduction of the arrival time of strains of low magnitudes is also to be remarked. Comparisons between solutions II and IV show that the last solution is in much better agreement with the experimental data than II.

Figure 5 shows the distribution of the maximum strain along the bar as furnished by II, IV–VI and the experimental data. The plateau near the impacted end is obtained for IV and V, but its length is much smaller than the one obtained with II. No plateau is described by VI.

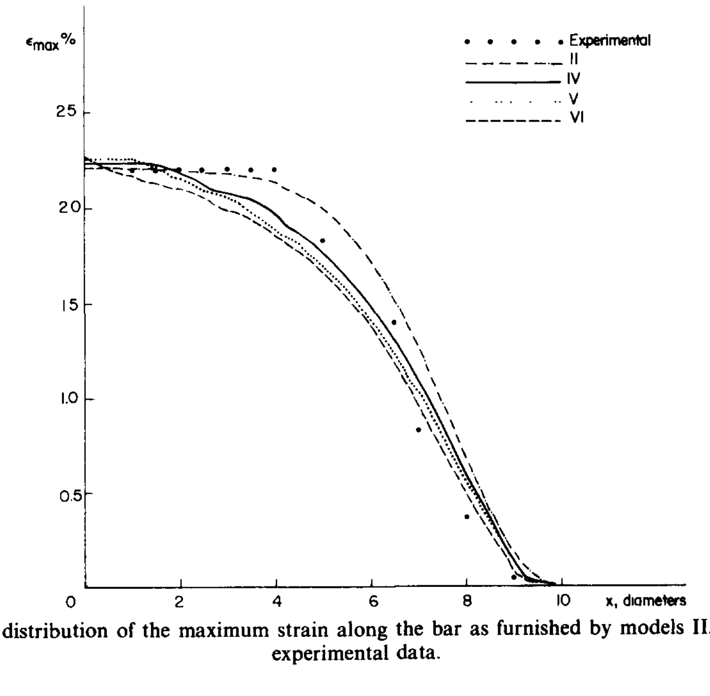

FIG. 5. The distribution of the maximum strain along the bar as furnished by models II, IV–VI and experimental data.

The stress–strain curves at various sections of the rod are shown in Fig. 6 for example IV and Fig. 7 for examples V and VI. These curves certainly cannot be compared with the experimental data but are, however, important for giving an insight in the behavior of the material at various sections of the bar. While the curves of Fig. 6 are nearly parallel on quite a long portion, those from Fig. 7 (dotted for example V and dashed for example VI)

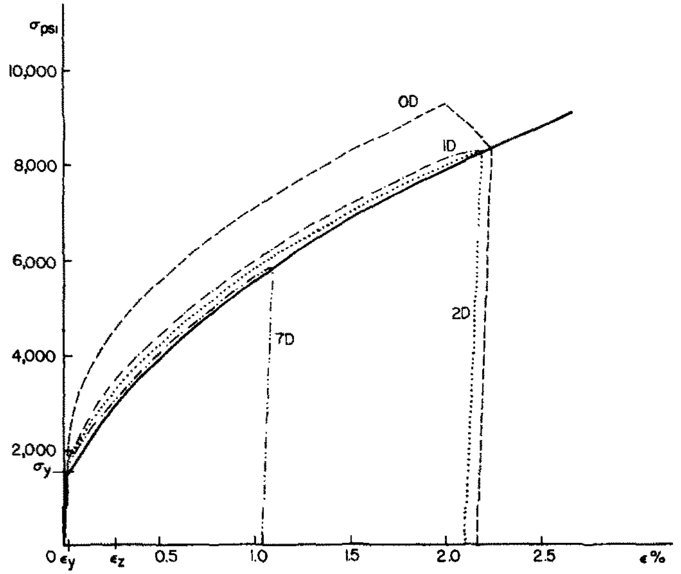

Fig. 6. Stress–strain curves at various sections of the bar, for example IV; the full line is the relaxation boundary.

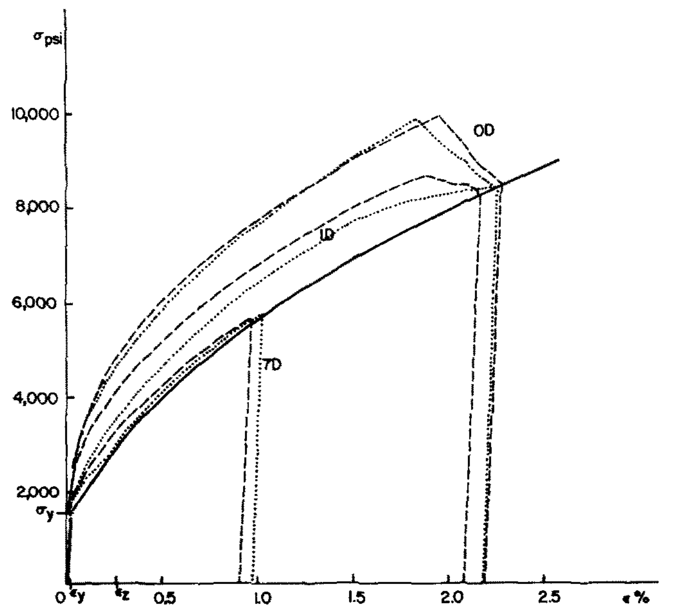

Fig. 7. Stress–strain curves at various sections of the bar for example V (dotted) and VI (dashed); the full line is the relaxation boundary.

are not. It is interesting to observe that by diminishing k the stress in all the sections of the bar is increased, while by decreasing Φ the stress is increased significantly only in the sections of the bar close to the impacted end. Generally for all cases the stress–strain curves at the sections close to the free end depart little from the solid curve representing the relaxation boundary (8); in fact it is only in the sections very close to the impacted end that the stress–strain curves depart significantly from (8).

The examples VII–IX have been obtained with some other expressions used for the functions Φ and Ψ (see Table 1). From the three mentioned examples the example VII is in a better agreement with the experimental data. Example VIII was computed with the same values of the constants for Ψ as in VII; however, one has made $\gamma = 0$, i.e. $\Phi = 0$. Thus a Malvern-type constitutive equation was used for this example. In example IX, again the values of various constants were the same as in VII except that for k a much smaller value was used. The aim was to consider two extreme cases where either the coefficient function Φ can be neglected (no time-independent plasticity), or the influence of the function Ψ is negligible during the impact because not enough time was allowed for the relaxation.

Example VII seems to furnish reasonably good agreement with the experimental data, at least in the first half of the bar. Now by making $\Phi = 0$ in example VIII the solution is deteriorated since: the lower portions of the strain–time curves are much too early, while at the upper part they are much too late; the maxima are slightly higher near the impacted end, but too low near the free end, the time of contact too small, etc. Therefore one obtains in a greater scale the effects reported already when passing from IV to V as shown in Fig. 2. When comparing IX with VII and the experimental data one can conclude that by drastically lowering the value of k all the strain maxima are dropped while the solution in the second half of the bar furnishes generally too low strains. The time of contact is drastically reduced.

The three solutions VII–IX furnish quite distinct variation laws of the stress at the impacted end of the bar (see Fig. 8). The solution VII provides a smaller initial peak stress

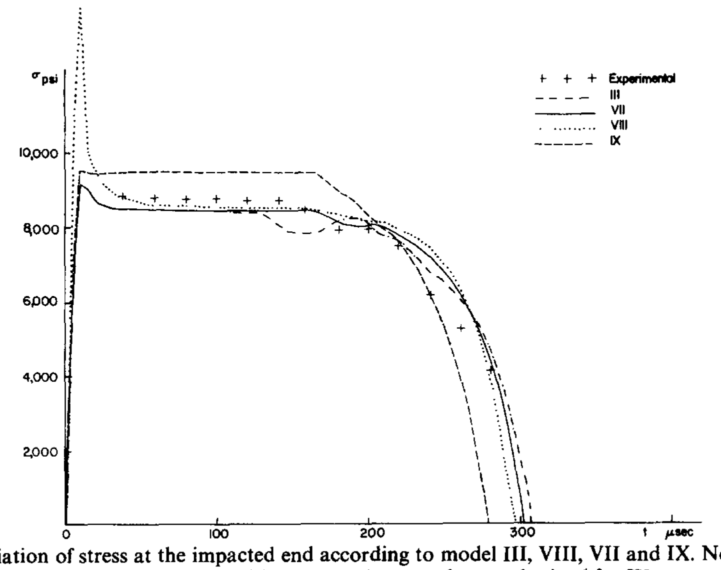

FIG. 8. Variation of stress at the impacted end according to model III, VIII, VII and IX. Note the high peak stress obtained for VIII and upper plateau obtained for IX.

than VIII and IX (this peak stress would be higher if the boundary conditions used would be "instantaneous") followed by a plateau, the same one as furnished by III, but longer, i.e. the unloading at the impacted end begins later on for VII than for III (no peak stress is described by III). Along this plateau there are very small variations of the stress which cannot be represented. The important decrease of the stress takes place after 160 μsec. The decrease slope is in rather fair agreement with the experimental data and is not really too much distinct from III. Solution VIII provides a much higher peak stress followed by a slightly higher plateau along which, however, the stress is steadily decreasing. Solution IX furnishes a negligible initial peak stress, but the plateau is at a much higher level. The decreasing portion of the curve is too early, so that the time of contact is much too small.

The stress–strain curves at various sections for VII (not given) are similar to those of example IV given in Fig. 6, all more or less parallel to the relaxation boundary. For example VIII (with $\Phi = 0$) this is no longer true, particularly near the impacted end where the peak stress shows up in the stress–strain curve (not given). Figure 9 shows the stress–strain curves for example IX (small k, long relaxation time) at $x = 0$, $1D$ and $7D$, all practically coinciding with the nonviscous instantaneous-response curve. It is remarkable that the falling portions of these curves, even above the relaxation boundary (solid curve in Fig. 9) appear to follow the elastic unloading line. Although this approximately straight-line portion is in fact in the relaxation region, where $\dot{\varepsilon}_P > 0$ very little plastic strain occurs during the time that the stress–strain point moves along it. This is because the relaxation time $1/k$ is so long. There are huge areas in the characteristic plane (not given here) corresponding to relaxation, i.e. the decreasing portion of stress–strain curves where

$$\dot{\sigma} < 0, \qquad \dot{\varepsilon} > 0, \qquad \dot{\varepsilon}_E < 0, \qquad \dot{\varepsilon}_P > 0 \tag{34}$$

(see [5, chapter III]) is reduced nearly to a point on each of these curves though (34) holds

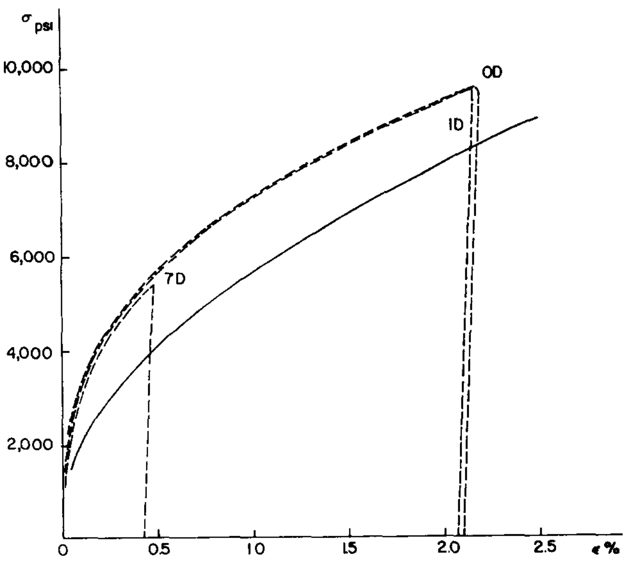

FIG. 9. The stress–strain curves at various sections of the bar are furnished by IX (small k); all curves are approaching the instantaneous response curve (21).

for a long period of time. The relaxation time is, however, much too long so that no significant stress relaxation takes place in the time intervals involved. For case IX the areas of the R-domains in the characteristic plane are even more significant than those of example VI, shown in Fig. 4.

Example X was computed by using the expression (9) into (7) and considering a variable k-coefficient according to (12), while for Φ the expression (15) has been used (see Table 1).

The model used in XII is slightly different from those used in the previous examples. Formulas (7), (10) and (12) have been used to define Ψ while in Φ besides (15) and (16) one has used (18) as well. This means that in a strip above (18) one will have still $\Phi = 0$ while from the upper boundary of this strip [defined by (8)] the function Φ may increase smoothly starting from zero. The threshhold imposed by the strip (18), below which there is no instantaneous plasticity may describe additional effects (these will be considered elsewhere). The results obtained with this model were quite close to those of example IV.

In the characteristic plane (not given), introducing the strip (18) enlarges the area of the R-domains while the L/R boundary is generally distinct from the R/U boundaries.

Another example, the XIIIth, was computed using the same model as in XII but with a smaller k. Decreasing k increases significantly the peak stress at the impacted end, while the decay is slow and slightly stepwise looking, so that the previous plateau practically disappears. The time of contact also becomes much too small.

The variation of the strain at $8D$ and $9D$ was obtained experimentally with electric resistance strain gauges, believed to be less accurate than the diffracting grating method. That is why less weight was granted to these measurements when trying to improve the model used. A short discussion, however, may still be useful for further improvement of the model. In Fig. 10 are shown the variations of strain at $8D$ as given by various models and the experimental data. For small strains the agreement is reasonable for several models. The best agreement is for XII, the only case shown at small strains. When strain surpasses ε_Y none of the curves is in good agreement with the experimental data. Two main disagreement points have to be noticed: all the computed solutions are too early at the rising portions and the maxima do not coincide with the experimental one. Considering various models used one may conclude that, at least partially, the first disagreement can be removed by raising the yield stress. A further improvement may be possible by rounding off the curve (8) in the vicinity of the yield stress.

The second disagreement point is impossible to match with the experimental data at $6{\cdot}5D$ and $7D$ (which were available). Thus for I and its rate-counterpart model XI the maxima at $8D$ are too low, but they are low at $7D$ as well and generally the solutions I and XI are in disagreement with the experimental data altogether.

The parameter k governs quite well the level of the maximum strain at $8D$. Thus for $k_o = 10\,\sec^{-1}$ (example IX) the maximum is too low, for $k_0 = 10^3\,\sec^{-1}$ (example XII) the maximum is too high while for $k_0 = 10^2\,\sec^{-1}$ (example XIII) the maximum coincides with the experimental one. However, for $k_0 = 10^2\,\sec^{-1}$ (example XIII) the maxima at $6{\cdot}5D$ and $7D$ are then too low while XII gives a perfect agreement at these two sections. By varying a little σ_Y or the expression of Φ (example X) one can still influence slightly the maximum. Example VIII gives also a good maximum at $8D$, but generally the overall agreement of solution VIII is poor.

To summarize, if one trusts the experimental maxima at $6{\cdot}5D$ and $7D$ then the theoretical solutions which fit reasonably these maxima will be too high at $8D$ and at $9D$ (not given

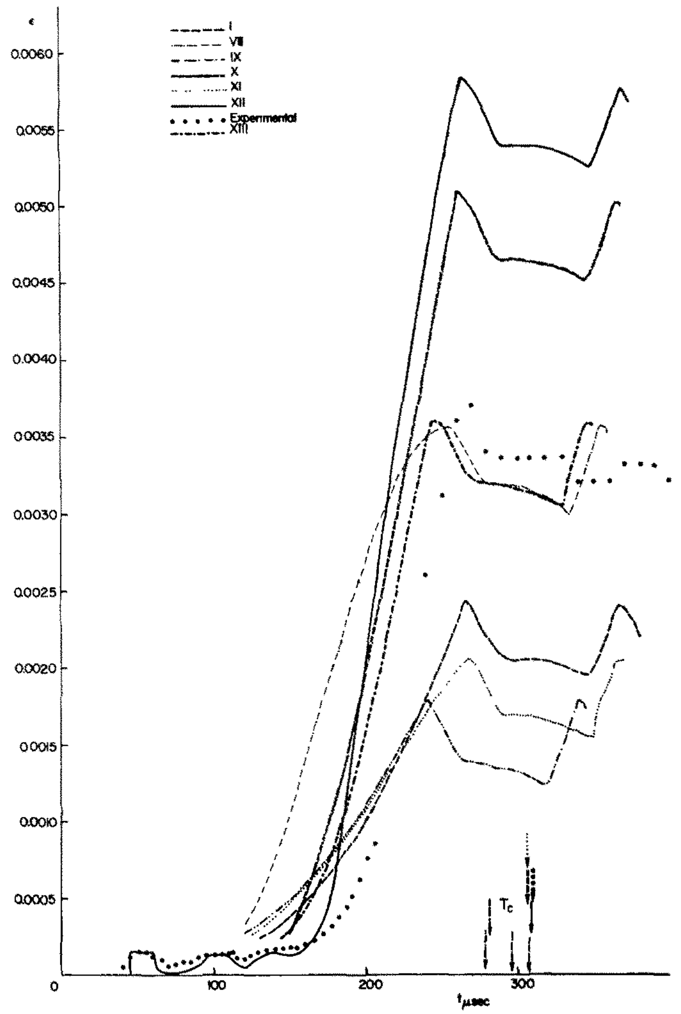

FIG. 10. Strain–time curves at $8D$ as furnished by various finite stress–strain laws, rate-type laws and experiment. the arrows are showing the time of contact for various cases.

here), while a good fit at $8D$ and $9D$ will give maxima much too low at $6{\cdot}5D$ and $7D$. This conclusion is true for both rate type and finite form type constitutive equation (see [2]).

PROCEDURE TO DETERMINE THE CONSTITUTIVE EQUATION

The examples exposed in the previous section enable us to give the details concerning the procedure to be used in order to find the expressions of various functions and constants entering the constitutive equation. One has to make precise that the aim of this paper was not to find constitutive equations which would fit perfectly with a certain set of experimental data, but rather to stress the procedure used in determining the constitutive equation. The experimental data were used as a starting point. The procedure could equally well be applied to other problems: torsional impact of thin-walled tubes, uniaxial strain problems, etc.

From all the experimental data at hand it is the ε–t curves at various sections of the bar to whom the greatest weight was conferred. The reason is that these curves were established with a very accurate experimental method (the Bell's diffraction grating technique). Second in importance is the variation of stress at the impacted end of the bar. All the other experimental data ($T_c, v_f, \bar{\varepsilon}, x_U$, ε–t curves obtained with elastic resistance strain gauges) were used only for an additional check of various models and of the description of the unloading process. It is evident that without a complete set of experimental data for the type of experiment considered, it is impossible to determine the constitutive equation.

The curve (8) is the first to be found. This is the curve in the σ–ε plane establishing for various velocities of impact the correspondence between magnitudes of the strain at the plateau and that of the stress at the corresponding plateau. That is why this curve was called relaxation boundary and may not generally coincide with the "static" stress–strain curve (see also Campbell [10]). Experimentally this curve can be obtained by measuring the stress plateau at the impacted end, or in a hard transmitter bar and the strain (or particle velocity) plateau in the first $\frac{1}{3}$ of the bar, near the impacted end. Thus one has to measure quite stable quantities: a constant stress in a quite long interval of time and a strain constant along a certain portion of the bar. Note that the stress plateau may in some cases be reduced to a very small one which follows the decay of the overstress and is located just before the significant dropping due to the unloading process. Thus in dynamic problems it is the relaxation boundary which is of great significance and not the "static" stress–strain curve.

The level of the stress-plateau (or that of the lower stress plateau if there are several) is governed mainly by the function $f(\varepsilon)$ in $\Psi(\sigma, \varepsilon)$. However, by making Φ smaller one can slightly raise the plateau. The same effect can be obtained by lowering k. If the decrease of k is significant, a second upper plateau or several intermediary plateaus distributed along a long decreasing stress slope may be formed.

The order of magnitude of k can significantly change the overall behavior of the solution. If k is "big" (for the examples considered $k > 10^4\,\text{sec}^{-1}$ would be rather "big") then the stress–strain relations at all the sections are very close to relaxation boundary and approach it from above. In order to avoid important computation errors it is useful to switch in this case to a stress–strain law written in finite form, where (8) would be just such a law. In this case the program for the computer is to be changed. If, however, k is very small (for the examples under consideration $k < 10\,\text{sec}^{-1}$ would be "small") then the stress–strain curves in all the sections are close to the instantaneous response curve (21) and approach it from below, so that again one can be tempted to switch to a stress–strain law written in finite form [an integrated form of (21) can be such a law]. In this latter case, however, one can well use a "rate" type of program, for a stress–strain curve written in finite form, but introduced in Φ and not in Ψ. This procedure is attractive since the program for rate-type constitutive equations is much easier to write than a program for a constitutive equation written in finite form.

Therefore by passing from rate to finite form theories one can go either to (8) by making $k \to \infty$ or to (21) by making $k \to 0$. For uniaxial stress or strain problems it is immaterial which procedure is used; the method used is a matter of convenience only. For combined-stress problems, however, things are changed in a fundamental manner: introduction of the yield condition in the Φ-terms will couple the plastic waves while introduction of the yield condition in Ψ-terms will not couple them (see [9]). One has to observe, however, that even for one-dimensional problems the two limit cases describe in a significantly different manner the unloading phenomena, so that experimentally one can distinguish easily which of the two procedures is to be followed if finite form theories are desired. The same is true for any generalization of the model for two or three dimensional cases. From a rational point of view it is the curve (21) obtained for $k \to 0$ which would correspond to the classical "time-independent" approach of plasticity theory and not the curve (8).

The previous discussion was done for say, an average range of rate of strain involved in such kinds of dynamic problems. Higher strain rates will lead to stress–strain curves closer to (21) while smaller strain rates to curves closer to (8). For instance in the previously mentioned examples in the sections near the impacted end (with higher strain rates) the stress–strain curves are higher and are followed by a significant decreasing portion where inequalities (34) hold (the strain dependent relaxation times are rather small) while in the sections near the free end a converse situation occurs (here the relaxation times are larger). Thus one has to be careful when trying to describe the behavior of the whole specimen during the entire experiment by a single "higher" stress–strain curve. It is also important to observe that when the rate of strain is decreasing, by a limit procedure one does not obtain the static stress–strain curve as behavior of the material but the relaxation boundary curve (8).

Some remarks concerning the coefficient function Φ. This is the coefficient controlling the velocity of propagation of the first part of the rising portion of the ε–t curves in the loading domain. Therefore Φ may be determined by measuring the arrival time of various levels of strain in the loading domain. This procedure will not furnish a unique expression for Φ. At the same time Φ evidently controls the level of the stress–strain curves; even more, with this function an upper boundary for the stress–strain curves can be introduced. Thus in order to uniquely determine Φ a stress measurement is also necessary. However, the following indirect procedure can also be suggested. The computed results showed in every case that at $x = 0$, when $\partial^2\varepsilon/\partial t^2 \leq 0$ we have $\Phi = 0$, so that the upper part of the ε–t curve (where $\partial^2\varepsilon/\partial t^2 < 0$) corresponds to the decreasing portion of the σ–ε curve at $x = 0$, when a dynamic creep and relaxation take place. In Fig. 11(a) the point P where

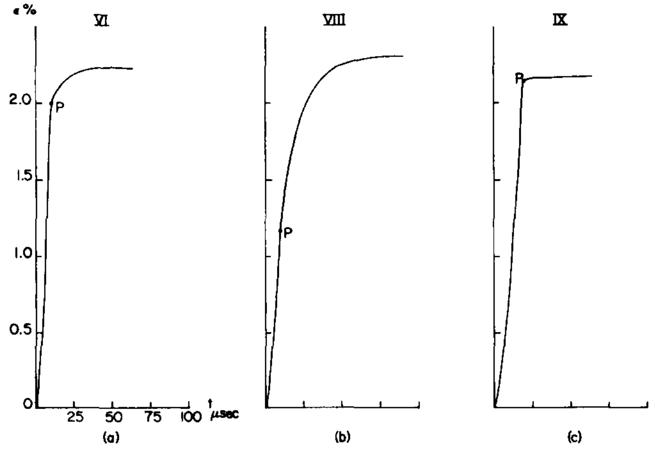

FIG. 11. The variation of strain at the impacted end as furnished by: (a) model IV; (b) model VIII and (c) the model with small value for k (IX). The point where curvature changes corresponds to the peak stress.

$\partial^2\varepsilon/\partial t^2 = 0$ corresponds to the peak stress shown in Fig. 6 for example IV. The same is true for the other cases. That is why for smaller Φ, when the σ–ε curves are higher, the relaxation period is longer, and the upper part of the ε–t curves where $\partial^2\varepsilon/\partial t^2 < 0$ is longer. It is only at $x = 0$ that $\partial^2\varepsilon/\partial t^2 = 0$ just at the peak of the stress–strain curve (when $\Phi = 0$); in the neighboring sections first the curve ε–t changes curvature and only for higher strain Φ becomes zero. For small k on the ε–t curves at $x = 0$ one has practically no portion where $\partial^2\varepsilon/\partial t^2 < 0$; the ε–t curves have the same kind of shape as those obtained with a finite stress–strain law [see Fig. 11(c)] i.e. these curves do not change curvature in the loading domain. For the case $\Phi = 0$ the point where curvature changes is very low [see Fig. 11(b)] in the sections of the bar very close to the impacted end. Thus the shapes of the upper part of the ε–t curves (above the point P) are to a great extent governed by the parameters $k(\varepsilon)$ and $\Phi(\sigma, \varepsilon)$: high values for k or small values for Φ will increase the length of this upper portion of the curve and vice versa. Thus, by obtaining the ε–t curves in some section of the bar close to the impacted end one can determine both Φ and k. Note that for semilinear models, the amplitude of the peak stress is governed by the loading regime at the boundary only.

CONCLUSIONS

There are some effects which can be described with rate type theories and cannot be described by finite form theories. For instance, model VI or XII can describe qualitatively (maybe that for perfect quantitative agreement with a certain set of experimental data, additional improvement of constants and functions entering the coefficients would still be necessary) the following experimentally observed effects (some of these effects may as well be influenced by some other phenomena, such as lateral inertia, etc.):

—the presence of the peak stress which decays within 10–15 μsec to the plateau in the first half diameter;
—the possible presence of an "overstress" (plateau or slowly decreasing slope);
—the change of curvature on the strain–time curves (see Fig. 2, for instance);
—the fact that strain very close to the impacted end is after 20 μsec lower than the maximum strain, while the stress is higher than that of the plateau;
—very close to the impacted end the maximum strains are higher while the plateau follows afterwards.

Some short remarks follow. A slightly higher yield stress than the static one introduced in (8) improves the solution mainly near the free end. From the plotting of the ε–t curves in the loading domain, using various rate-theories, one has obtained the well-known property assumed a long time to be valid for finite stress–strain relations only: a certain level of strain propagates with an apparently constant speed. The "perfect elastic" unloading seems to be a reasonably good description of the unloading process for the constitutive equations considered.

A final remark: since the so-called "rate-effects" are significant mainly near the impacted end, any estimation of the behavior at the impacted end using the observed behavior along the bar is questionable.

Acknowledgments—The author wishes to express his appreciation to L. E. Malvern for reading the manuscript and offering many valuable suggestions and to Cornelia Cristescu for writing the program in FORTRAN IV and taking care of the computations. The computations were done at the Computing Center of the University of Florida for which the author is grateful to the Department of Engineering Science and Mechanics.

REFERENCES

[1] N. Cristescu, The unloading in symmetric longitudinal impact of two elastic–plastic bars. *Int. J. Mech. Sci.* **12**, 723 (1970).

[2] N. Cristescu and J. F. Bell, On Unloading in the Symmetrical Impact of Two Aluminum Bars, *Inelastic Behavior of Solids*. McGraw-Hill (1970).

[3] J. F. Bell, *The Physics of Large Deformation of Crystalline Solids*. Springer-Verlag (1968).

[4] N. Cristescu, The Influence on the Plastic Wave Propagation of the Variation of Young's Modulus with Plastic Strain, *Proceedings of the First International Conference on Structural Mechanics in Reactor Technology*, Berlin (1971).

[5] N. Cristescu, *Dynamic Plasticity*. North Holland (1967).

[6] N. Cristescu, On the propagation of elastic–plastic waves in metallic rods. *Bul. Acad. Pol. Sci.* **XI**, 129 (1963).

[7] L. E. Malvern, The propagation of longitudinal waves of plastic deformation in a bar of material exhibiting a strain rate effect. *J. appl. Mech.* **18**, 203 (1951).

[8] J. F. Bell, Study of initial conditions in constant velocity impact. *J. appl. Phys.* **31**, 2188 (1960).

[9] N. Cristescu, On the coupling of plastic waves as related to the yield condition. *Rev. Roumaine Sci. Techn., Ser. Mec. Appl.* **16**, 797 (1971).

[10] J. D. Campbell and R. H. Cooper, private communication.

(*Received* 21 *June* 1971; *revised* 13 *September* 1971)

Абстракт—Выходя из экспериментальных данных, приводится способ определения разных функций и постоянных, которые появляются в конститутивном уравнении, описывающим как пластичность, зависящую от времени, как и независящую. В среди типичных экспериментов приводится один, а лично симметрический продольный удар двух техже самых стержней, в виду того, что этого рода задачи дают большое количество экспериментальных данных.

Рассматривается, также, процесс разгрузки, для того, что в основном во время разгрузки можно выяснить интересные аспекты, касающиеся "пластичности". Выводятся "границы релаксации", которая играет главную роль в пластиуности, зависящей от времени. Даются некоторые числовые примеры, для указания влияния разных функций или постоянных, существующих в конститутивном уравнении.